Supporting Information:

Concurrent activation of CO_2 and H_2O on sulfur-doped CNTs supported nickel phthalocyanine for electrochemical CO_2 reduction to CO

Abdulhadi Mustapha[a,b], Shanyong Chen[a,c,*], Jiaqi Xiang[a], Yifan Jiang[a], Jingyu Wang[a], Xiaojun Zhao[a], Fei Chen[a], Maoyu Wang[d], Hua Zhou[d], Ke Zeng[a], Linlin Wu[a], You-Nian Liu[a,*]

a Hunan Provincial Key Laboratory of Micro & Nano Materials Interface Science, College of Chemistry and Chemical Engineering, Central South University, Changsha, Hunan 410083, PR China.

b Department of Chemistry, Faculty of Science, Yusuf Maitama Sule University, Kano, Nigeria.

c Guangdong Key Laboratory of Environmental Pollution and Health, School of Environment, Jinan University, Guangzhou 511443, PR China.

d X-ray Science Division, Argonne National Laboratory, Lemont, IL, 60439, United States.

* Corresponding authors: Phone/Fax: 86-731-8887 9616

E-mail: shanyongchen@csu.edu.cn (S. Chen); liuyounian@csu.edu.cn (Y.-N. Liu).

1. Experimental

1.1 Chemicals

Nickel phthalocyanine (NiPc), polytetrafluoroethylene (PTFE), sulfur particles, *N,N*-dimethylformamide (DMF), Nafion solution, nitric acid, deuterium oxide (D_2O), and potassium sulfate were procured from Sigma-Aldrich (Shanghai, China). Gases including nitrogen, argon and carbon monoxide, each with a purity of 99.99% were sourced from Saizhong Gas (Changsha, China). All chemicals were analytical grade and were used as received without further treatment. Additionally, carbon nanotubes (CNTs) were purified by nitric acid treatment to remove impurity.

1.2 Preparation of S-doped CNTs

The preparation began with commercially available carbon nanotubes as a starting carbon material. Initially, CNTs powder (0.5 g) was mixed with HNO_3 solution (6 M, 200 mL) in a round bottom flask. This mixture was heated to 80 ^oC for 24 h in a reflux setup. Afterward, the acid treated CNTs was collected by centrifugation, and then thoroughly rinsed with deionized water and absolute ethanol until a neutral pH level is reached, followed by drying in an oven at 80 ^oC overnight. The resulting product was grounded into a fine powder. S-CNTs was prepared by annealing a mixture of sulfur particles and purified CNTs (weight ratio 1:10) at 750 ^oC under Ar flow for 2 h.

1.3 Preparation of NiPc/S-CNTs catalyst

To prepare the NiPc/S-CNTs catalyst, nickel phthalocyanine (8 mg) and S-CNTs (100 mg) was dispersed in dimethylformamide (DMF, 50 mL). The solution underwent ultrasonic treatment for 1 h, followed by 24 h of magnetic stirring at room temperature. The resulting NiPc/S-CNTs hybrid was then isolated by centrifugation and dried in a vacuum oven at 60 ^oC for 12 h. A similar experimental method was adapted for the preparation of NiPc/CNTs, in which S-CNTs was replaced by CNTs.

1.4 Electrochemical measurements

The electrochemical performances of the newly prepared NiPc/S-CNTs catalysts were assessed in a three-electrode flow cell system utilizing a Wave Driver 100 (Pin Research Instrument, USA). In this setup, carbon paper strips (1 cm × 3 cm) were used as the working electrode, Ag/AgCl served as the reference electrode, and Ti functioned

as the counter electrode. To formulate the catalyst ink, the catalyst (6 mg) was dissolved in a solution containing ethanol (2200 μL), nafion (5 wt%, 100 μL), and PTFE (5 wt%, 200 μL). The resulting suspension was subjected to ultrasonication at room temperature for 30 minutes. The carbon cloth was coated with the ink (50 μL) during each drop-casting addition, and it was then dried at 50 ^{o}C for 10 min under an infrared lamp. This drop-casting process was repeated until the catalyst loading reached 0.75 mg cm^{-2}. An anion-exchange membrane separated the anodic and cathodic chambers, and the electrolyte (0.25 M K_2SO_4) in both chambers was pumped out at a rate of 10 mL min^{-1}. Before initiating electrochemical CO_2 reduction experiments, high-purity CO_2 gas (99.999%) was bubbled into the aqueous electrolyte to saturate the solution. The flow rate of CO_2 was maintained at 20 mL min^{-1} throughout the CO_2 reduction experiment, regulated using a gas mass flow meter. The resulting CO and H_2 products generated during CO_2 conversion were quantitatively analyzed using an online gas chromatograph (Agilent, model 7890B). The proportions of H_2 and CO were determined using a thermal conductivity detector (TCD) and a flame ionization detector (FID) equipped with a methanizer. High-purity N_2 gas (99.999%) served as the carrier gas. Liquid products were quantified using 1H nuclear magnetic resonance spectroscopy (^{1}H NMR). The faradaic efficiency of the gaseous phase products was accurately calculated based on the chromatograph peak and the equation (1) provided below.

$$FE_{CO\ or\ H_2} = \frac{2FP_0}{iRT}Vx \qquad (1)$$

Where *V* represents the flow rate of CO_2, *P*o denotes normal atmospheric pressure (100 kPa), *x* signifies the fraction of products, R is the molar gas constant, *i* stands for the applied current, *T* is the ambient temperature (298 K), and F represents the faraday constant (96485 C^{-1}).

1.5 Materials characterization

The X-ray photoelectron spectra (XPS) of the prepared catalysts were examined using an ESCALAB 250Xi X-ray photoelectron spectrometer (ThermoFisher-VG Scientific, USA). For X-Ray diffraction (XRD) analysis, a Bruker D8 diffractometer was utilized (Bruker, Germany). The surface structure of the catalysts was thoroughly

examined by scanning electron microscopy at 10 kV (SEM, Regulus8100, Hitachi, Japan), and transmission electron microscopy alongside high-resolution (HRTEM) using an FEI Tecnai-G2 F30 with an acceleration voltage of 300 kV (FEI, USA). Ultraviolet photoelectron spectroscopy (UPS) spectra were collected using ESCALAB 250Xi (Thermo Fisher). Raman spectroscopy (Renishaw in Via Raman microscope, UK) and an inductively coupled plasma atomic emission spectrometer (ICP-AES, Varian 710-ES) were employed to investigate the microstructure and elemental composition. The XAFS was measured at beamlines 5BM-D and 9-BM-B&C at the Advanced Photon Source of Argonne National Laboratory and obtained spectra were analyzed by utilizing Athena and Artemis software. Additionally, ^{1}H nuclear magnetic resonance spectroscopy (^{1}H NMR) data was acquired using an AVANCE 400-MHz NMR instrument (Buker, USA), Fourier-transform infrared spectroscopy (FTIR) spectra were recorded on a Scientific Nicolet is20 FT-IR spectrometer (Thermo Fisher). The CO_2 TPD spectrum was acquired using the PCA-1200 chemical adsorption analyzer (Beijing Construction Electronic Technology, China). The test temperature of CO_2-TPD ranges from 100 to 500 °C with the increasing temperature rate of 10 °C/min and the CO_2 adsorption is performed at 50 °C for 1 h.

1.6 *In situ* attenuated total reflectance surface-enhanced infrared absorption spectroscopy (ATR-SEIRAS) measurements.

In situ ATR-SEIRAS experiments were carried out using a Scientific Nicolet is20 FT-IR spectrometer (Thermo Fisher) equipped with an MCT detector cooled by liquid nitrogen. The silicon prism (20 mm diameter) plated with gold and catalyst was used as working electrode. The reference electrode was Ag/AgCl, and the counter electrode was Pt wire. The experiment was implemented in a CO_2-saturated 0.25 M K_2SO_4 solution, with the potential varied stepwise from 0.5 to 1.7 V (*vs*. Ag/AgCl). The spectrum obtained at the open circuit voltage was utilized for background subtraction.

1.7 DFT calculation.

All the first-principles spin-polarized calculations were implemented through employing plane-wave density functional theory (DFT) as assisted by the Vienna Ab Initio Simulation Package (VASP).[1, 2] The Perdew-Burke-Ernzerhof (PBE) formula

analyzing via projected augmented wave (PAW) method within the generalized gradient approximation (GGA) was used to cope with exchange-correlation potential.[3] The value of cut-off energy was fixed at 500 eV for all calculations. All the positions of atoms were fully relaxed until the Hellmann-Feynman forces on each atom were less than 0.01 eV/Å. The single-wall nanotubes of CNTs and S-CNTs models were constructed based on N=M=8 with a vacuum region of up to 20 Å along the a- and b-direction to avoid the interaction between adjacent layers. Meanwhile, the Brillouin zone is sampled with 2 × 2 × 1 Monkhorst-Pack k-points. The DFT-D3 method designed by Grimme is adopted to describe the van der Waals interactions, which has been demonstrated to accurately depict chemisorption and physisorption properties on layered material.

To examine the reaction free energy of intermediates (ΔG) at the catalyst (*) surface in CO_2RR process, the following equations were employed:

$$\Delta G_1 = (E_{COOH*} - 0.5\times E_{H2} - E_{CO2} - E_*) + (ZPE_{COOH*} - 0.5\times ZPE_{H2} - ZPE_{CO2} - ZPE_*) - T\times (S_{COOH*} - 0.5\times S_{H2} - S_{CO2} - S_*) \quad (2)$$

$$\Delta G_2 = (E_{CO*} + E_{H2O} - 0.5\times E_{H2} - E_{COOH*}) + (ZPE_{O*} + ZPE_{H2O} - 0.5\times ZPE_{H2} - ZPE_{COOH*}) - T\times (S_{CO*} + S_{H2O} - 0.5\times S_{H2O} - S_{COOH*}) \quad (3)$$

Where, E, ZPE and S are the total energy, zero-point energy, and entropy of intermediates, respectively. The thermal-correction energies for each intermediate at 298.15 K.

The transition state in the H_2O dissociation process is searched by the climbing image-nudged elastic band (CI-NEB) method[4,5], and the energy barrier of H_2O is calculated as follows: $E_a = E_{TS} - E_{H2O*,}$ where, E_{TS}, E_{H2O*} is the electronic energy of transition state and H_2O*.

1.8 Calculation of the coverage of the electrochemically active Ni site

The coverage of the electrochemically active Ni site (Γ) is calculated using the formula.[6]

$$\Gamma = \frac{(\frac{i_{p,c}}{v})\chi}{n^2 A} \quad (4)$$

Where, $i_{p,c}$ donates the cathodic peak current, v represent the scan rate, n gives the number of transferred electrons (which is n=1 for the $Ni^{2+} \rightarrow Ni^{+}$ redox peak), A is the electrode area, x is the constant,

$$x = \frac{4RT}{F^2} \quad (5)$$

Where, T is the temperature (298 K). R is the molar gas constant (8.314 J mol^{-1} K^{-1}), and F signifies the Faraday constant (96485 C mol^{-1}).

2. Supplementary Figures

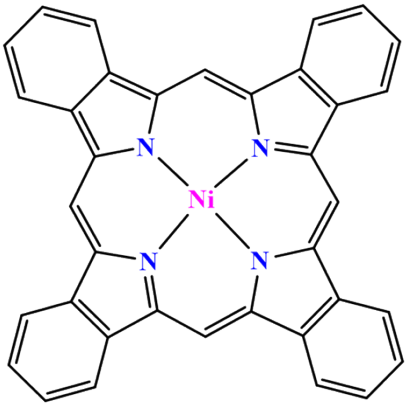

Figure S1. Structure of the nickel phthalocyanine (NiPc).

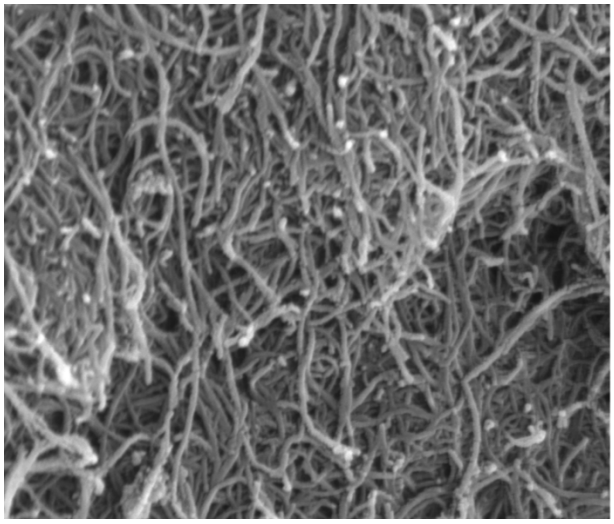

Figure S2. SEM image of NiPc/S-CNTs.

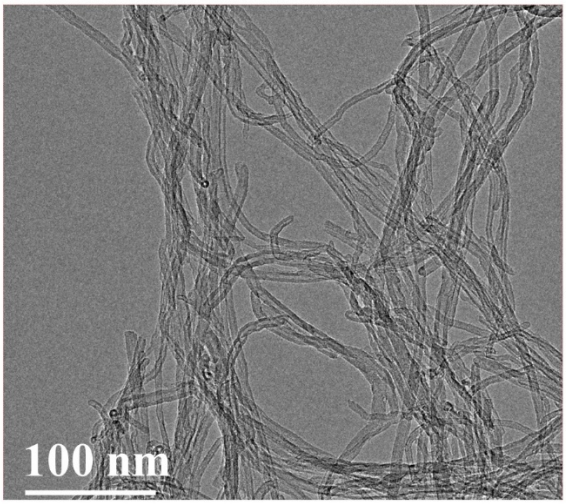

Figure S3. TEM image of NiPc/S-CNTs.

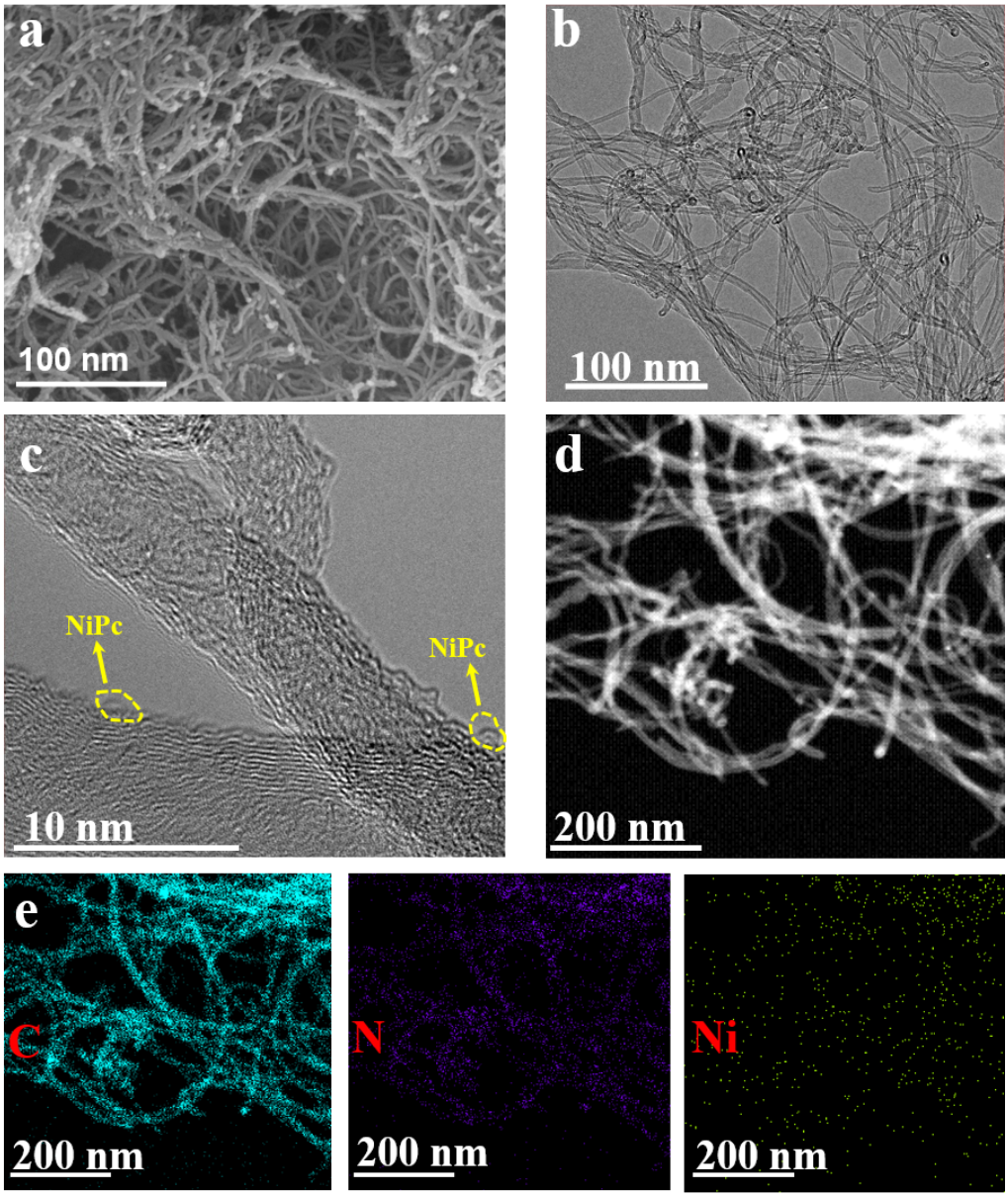

Figure S4. (a) SEM image of NiPc/CNTs. (b) The TEM image of NiPc/CNTs. (c) The HRTEM image of NiPc/CNTs. (d) HAADF-STEM image of NiPc/CNTs. (e) EDX elemental mapping images of C, N and Ni elements of NiPc/CNTs.

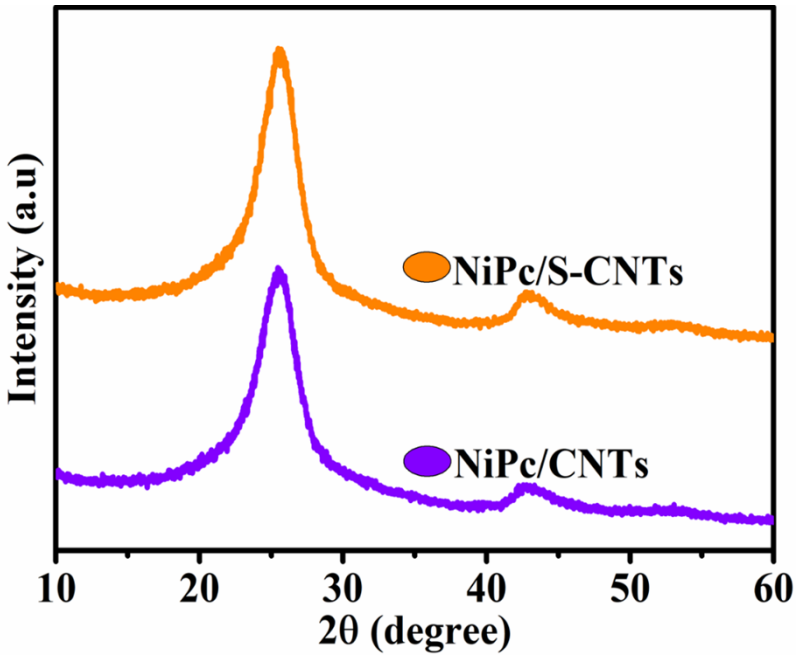

Figure S5. XRD patterns of NiPc/S-CNTs and NiPc/CNTs composite catalysts.

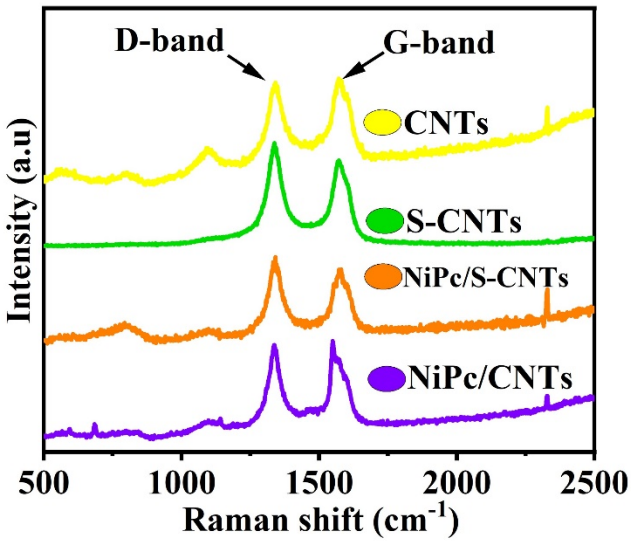

Figure S6. Raman spectra of NiPc/S-CNTs, NiPc/CNTs, S-CNTs, and pure CNTs.

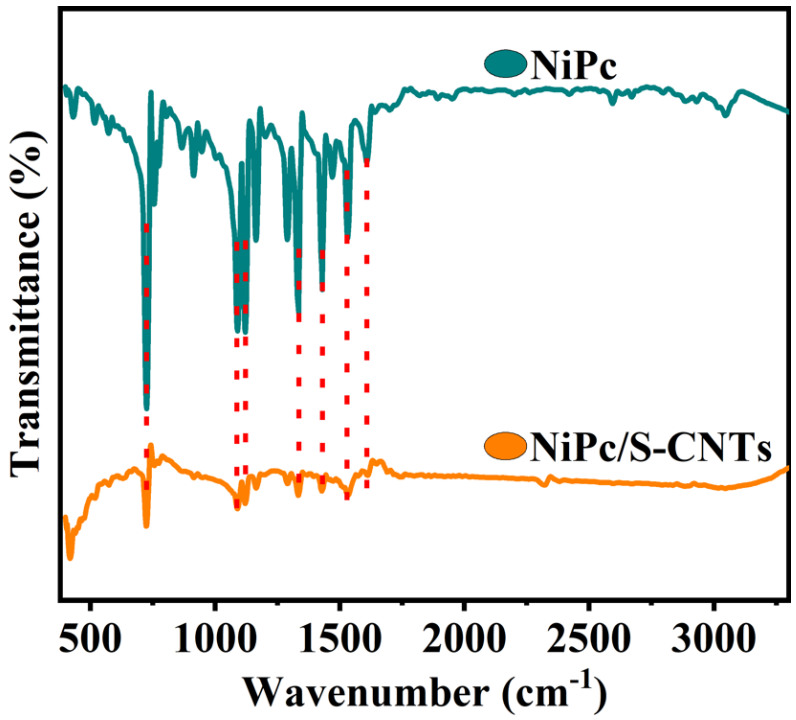

Figure S7. FT-IR spectra of NiPc/S-CNTs and NiPc/CNTs.

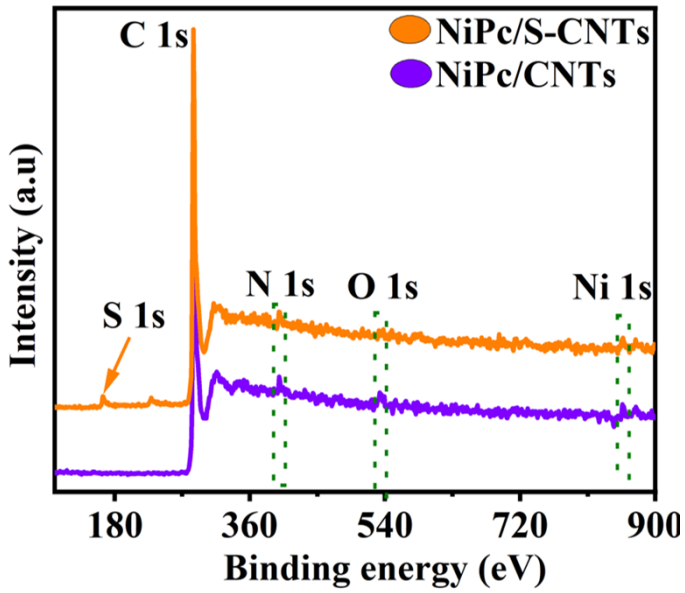

Figure S8. XPS survey spectra of NiPc/S-CNTs and NiPc/CNTs.

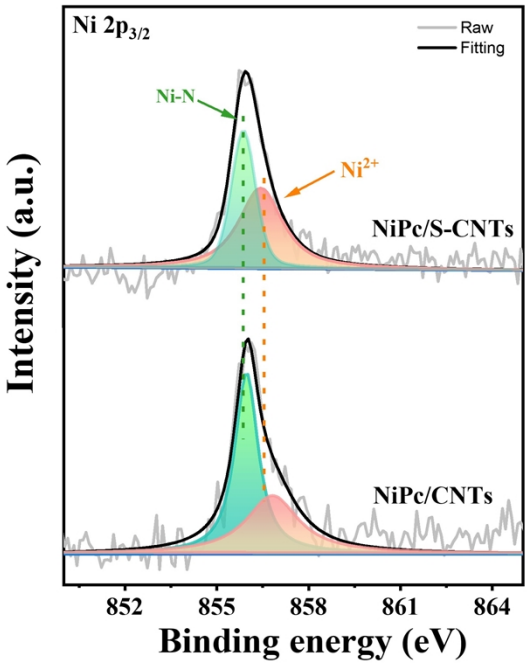

Figure S9. Raw and fitted XPS spectra of Ni $2p_{3/2}$ for NiPc/S-CNTs and NiPc/CNTs.

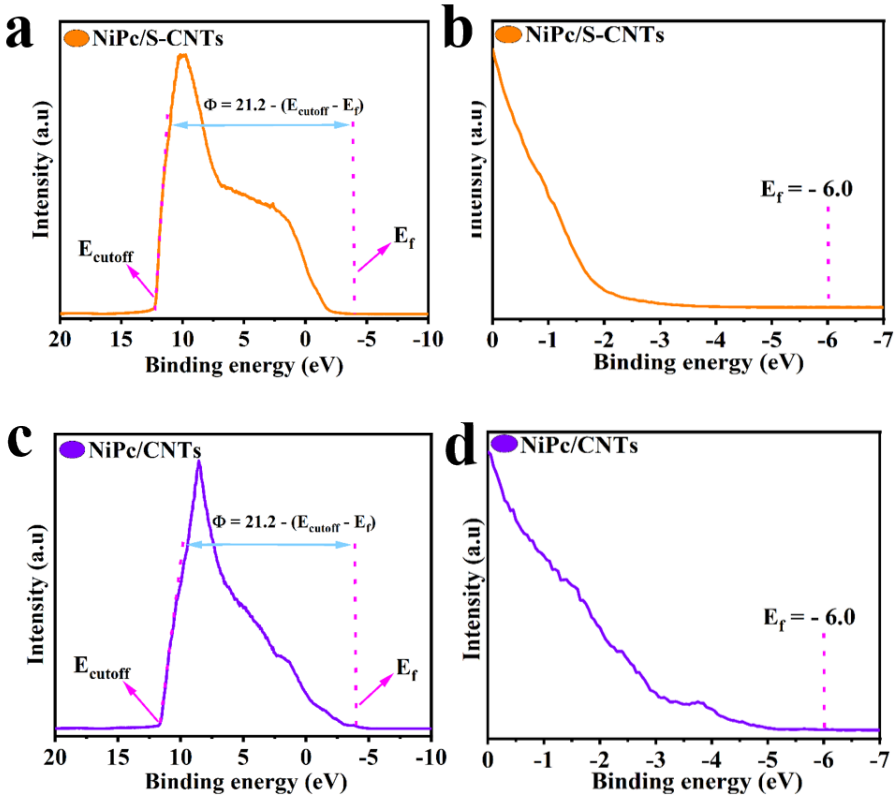

Figure S10. (a) UPS spectra of NiPc/S-CNTs, and (b) UPS spectra of NiPc/S-CNTs in the regions of onset (E_f). (c) UPS spectra of NiPc/CNTs, and (d) UPS spectra of NiPc/CNTs in the regions of onset (E_f). The work function, denoted as (Φ), can be calculated using the equation $\Phi = 21.2 - (E_{cutoff} - E_f)$.

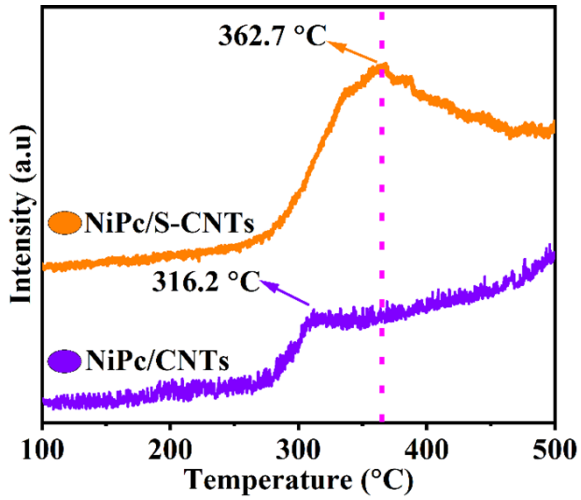

Figure S11. TPD curves of NiPc/S-CNTs and NiPc/CNTs.

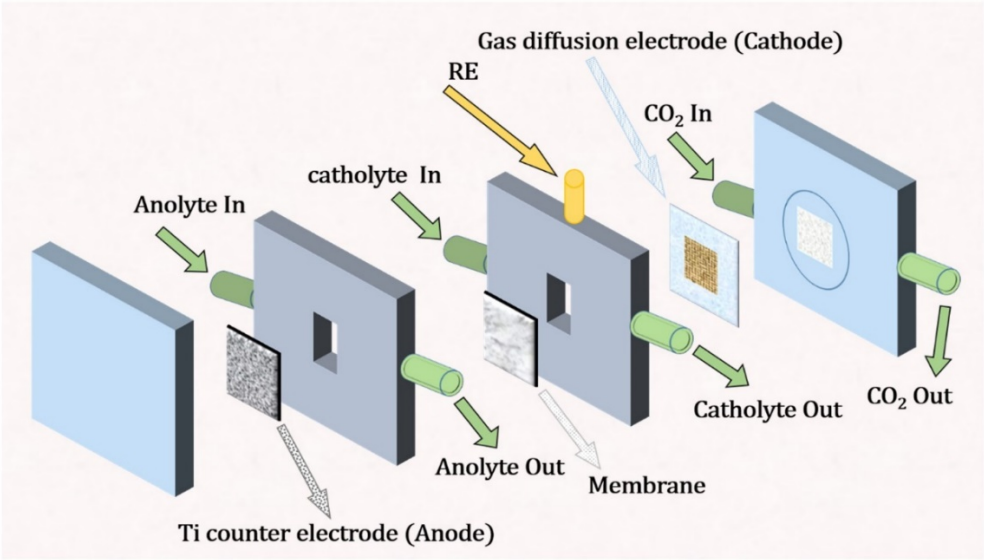

Figure S12. Schematic illustration of the flow cell for eCO_2RR.

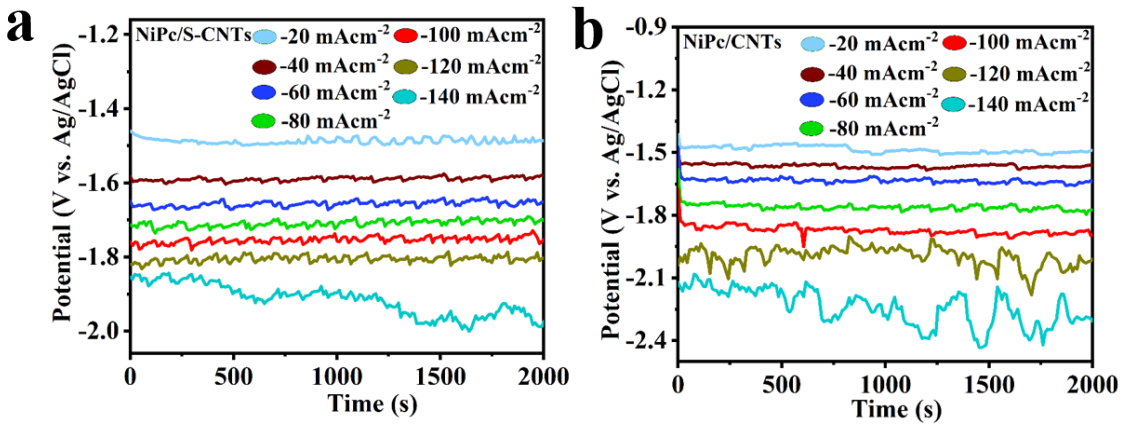

Figure S13. Chronopotentiometric measurement of (a) NiPc/S-CNTs and (b) NiPc/CNTs performed at different current densities in 0.25 M K_2SO_4 electrolyte.

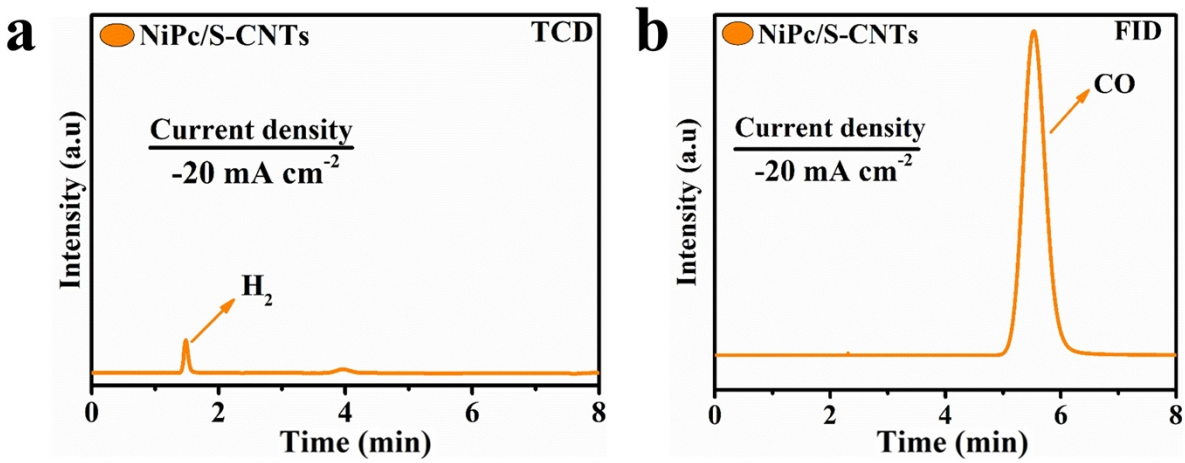

Figure S14. (a) and (b) GC traces depicting the gaseous products of NiPc/S-CNTs at –20 mA cm^{-2} from FID and TCD channel, respectively.

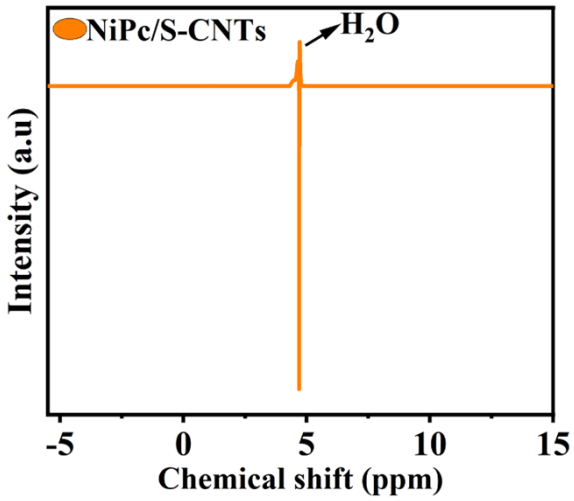

Figure S15. Liquid ^{1}H NMR spectrum of NiPc/S-CNTs.

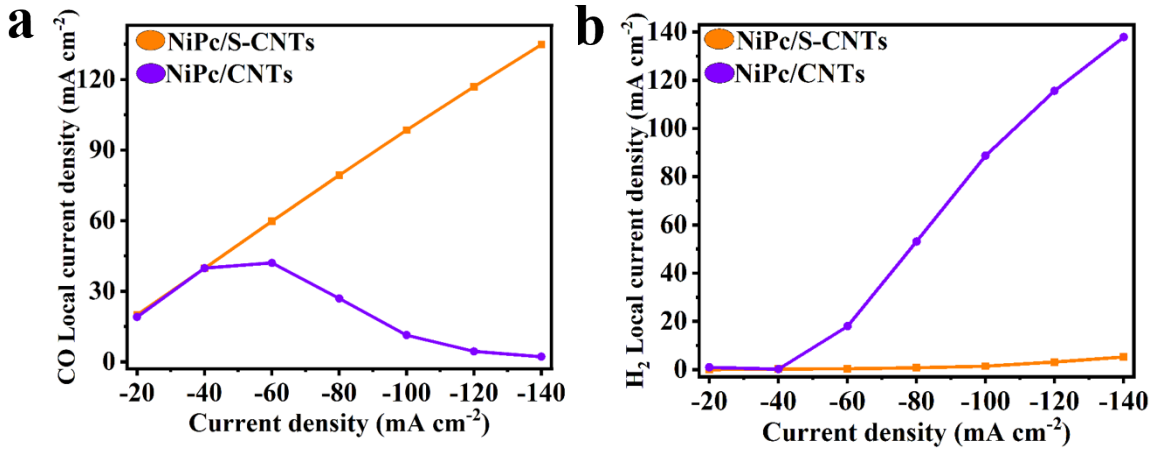

Figure S16. (a) CO local current density and (b) H_2 local current density of NiPc/S-

CNTs and NiPc/CNTs hybrid catalysts at different current densities.

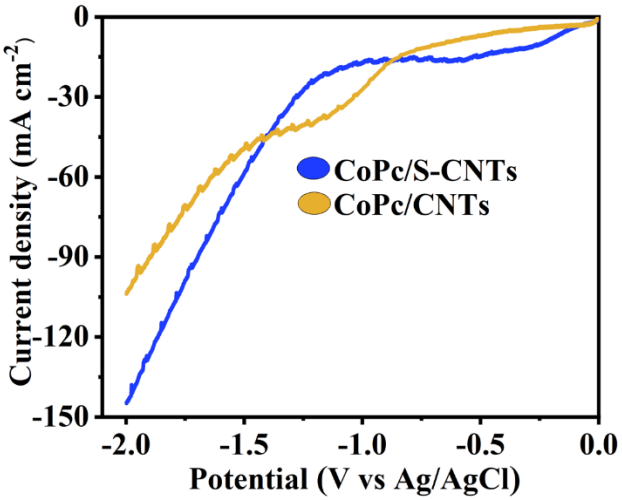

Figure S17. LSV profiles of CoPc/S-CNTs and CoPc/CNTs in CO_2-saturated 0.25 M K_2SO_4.

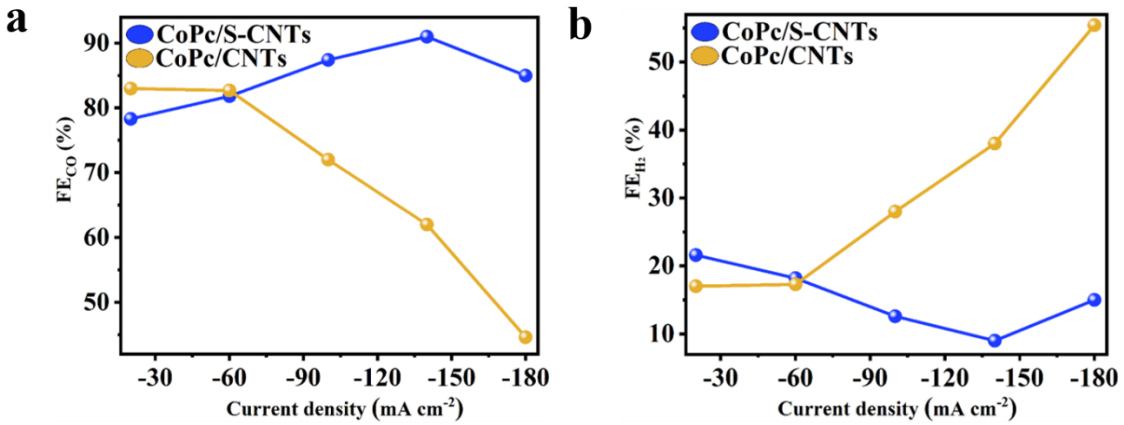

Figure S18. (a) FE_{CO} and (b) FE_{H_2} of CoPc/S-CNTs and CoPc/CNTs at different current densities.

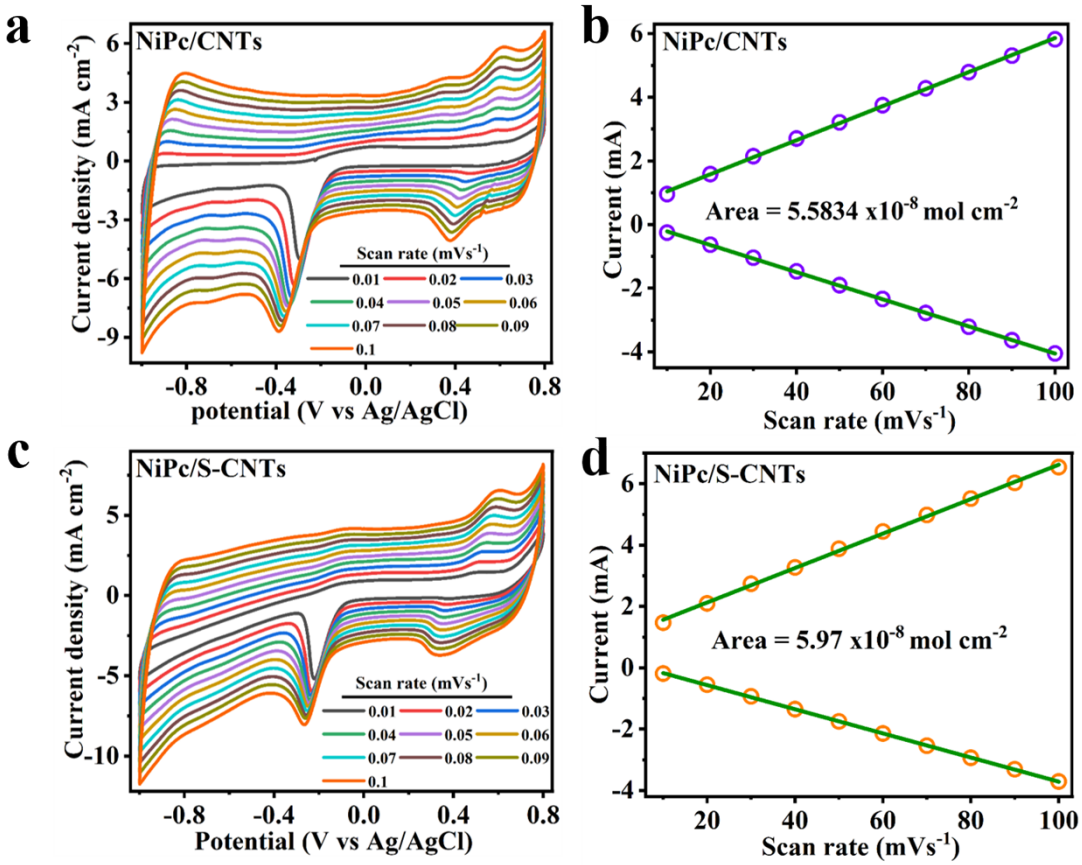

Figure S19. Ni^{2+}/Ni^{+} redox curves of (a) NiPc/S-CNTs and (b) NiPc/CNTs recorded with the scan rate from 10 to 100 mV s^{-1}, (c) and (d) the plot of the anodic and cathodic peak current densities of Ni^{2+}/Ni^{+} redox peak against the scan rates.

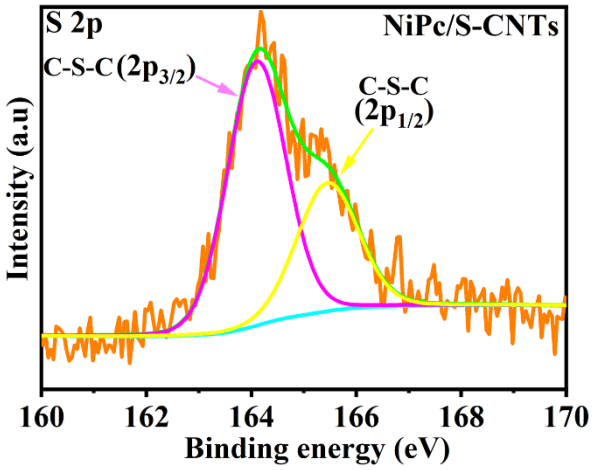

Figure S20. High resolution S2p XPS spectrum of NiPc/S-CNTs after eCO_2RR stability test.

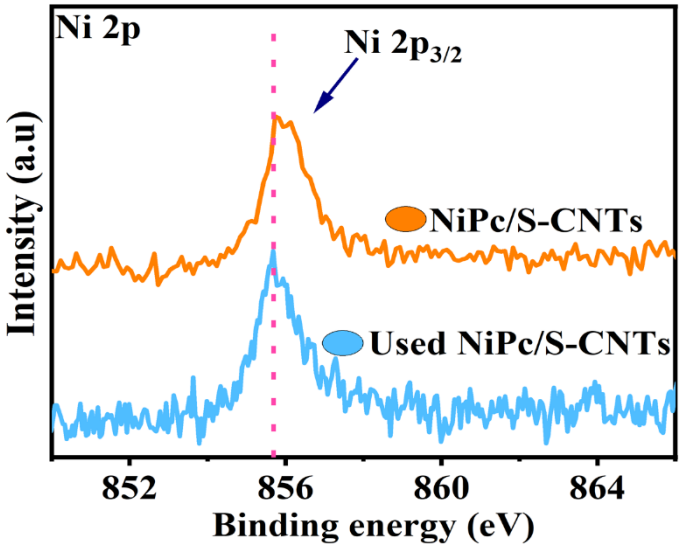

Figure S21. High resolution Ni 2p XPS spectrum of NiPc/S-CNTs after eCO_2RR stability test.

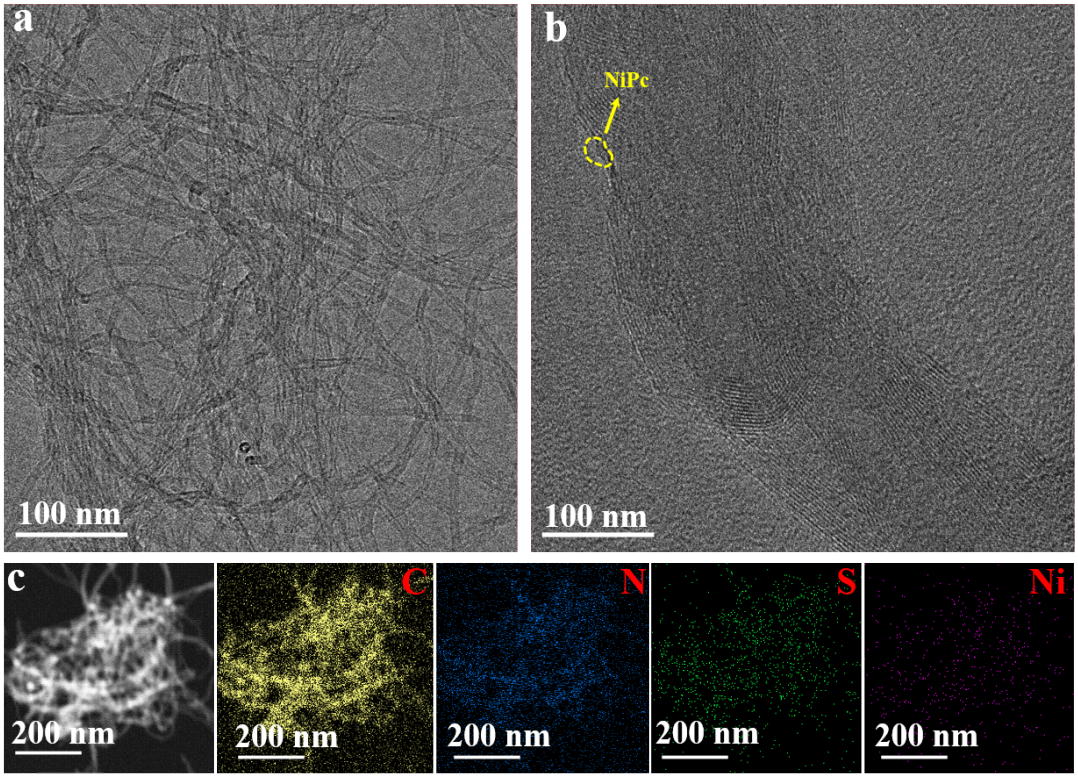

Figure S22. (a) TEM image of NiPc/S-CNTs after eCO_2RR stability test. (b) HRTEM image of NiPc/S-CNTs after eCO_2RR stability test. (c) EDX elemental mapping images of S, Ni, N and C elements of NiPc/S-CNTs after eCO_2RR stability test.

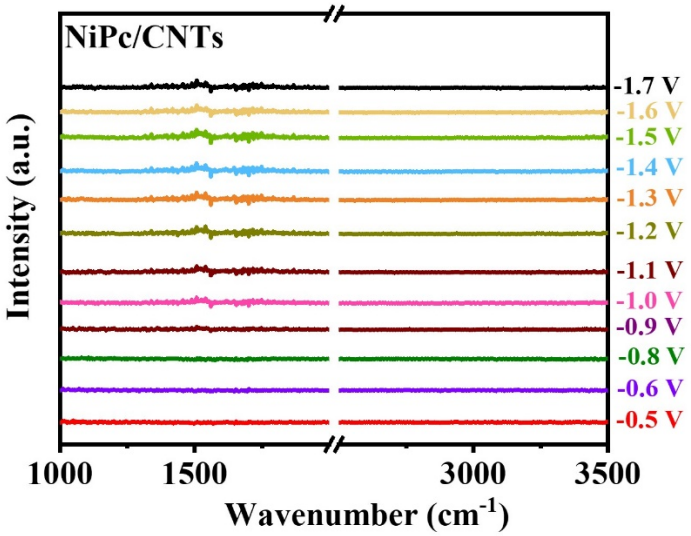

Figure S23. *In situ* ATR-SEIRAS spectra of NiPc/CNTs at different applied potentials (*vs*. Ag/AgCl).

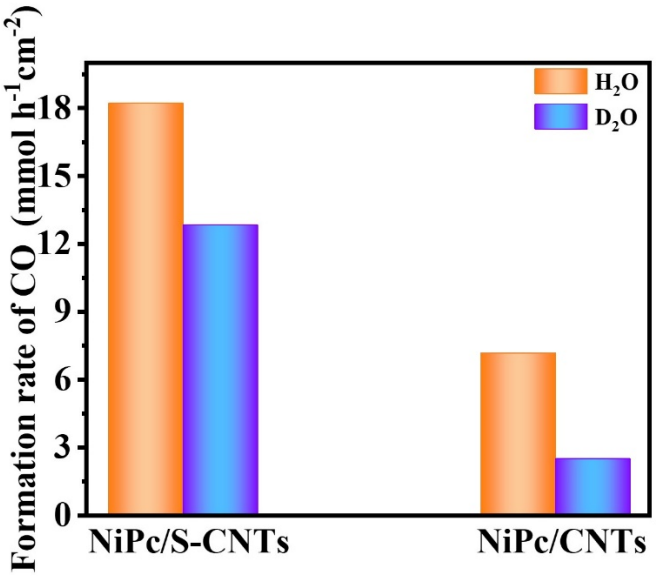

Figure S24. CO formation rate of NiPc/CNTs and NiPc/S-CNTs performed at –1.3 V (vs. Ag/AgCl).

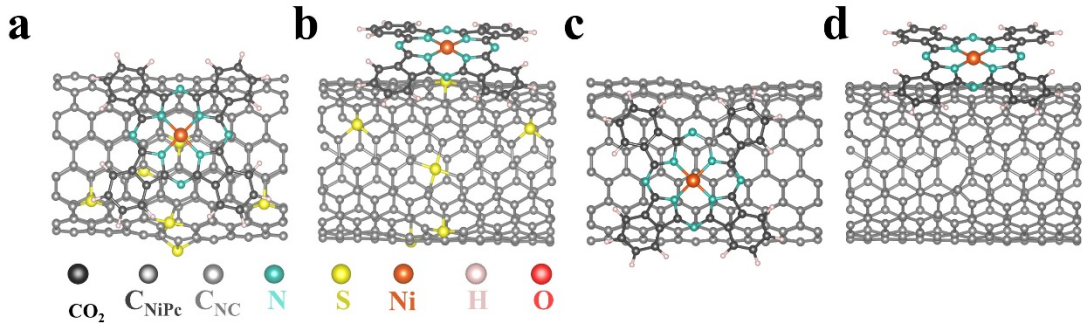

Figure S25. (a-b) Theoretical model of NiPc/S-CNTs. (c-d) Theoretical model of NiPc/CNTs.

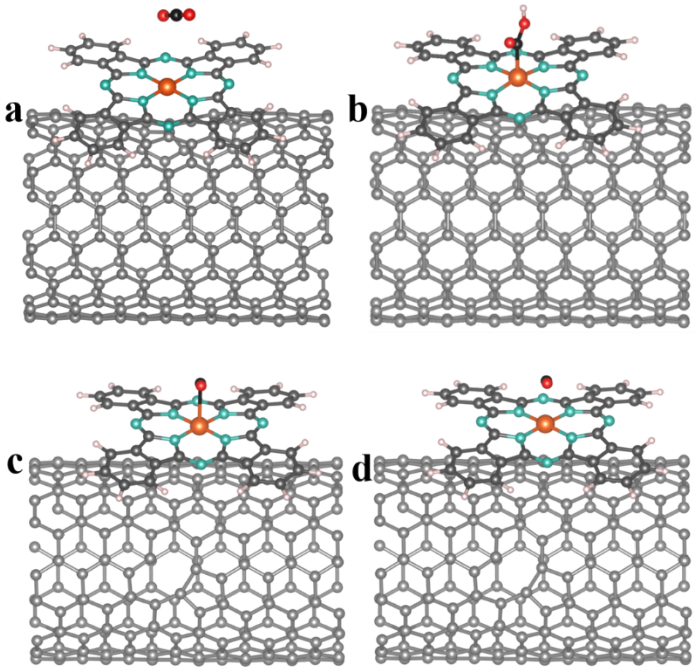

Figure S26. Theoretical model of NiPc/CNTs (a) prior to adsorbing CO_2. (b) When *COOH is adsorbed on Ni site. (c) When *CO is adsorbed on Ni site. (d) After releasing CO from Ni site.

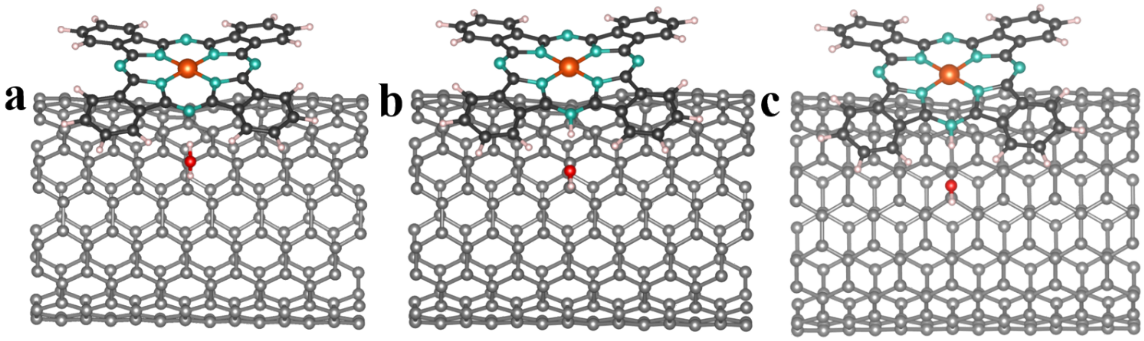

Figure S27. Theoretical model of NiPc/CNTs. (a) When *H_2O is adsorbed. (b) When H_2O is transformed to transition state (*H…OH). (c) After releasing H^+.

References

1. G. Kresse, et al., *Phys. Rev. B.*, 1993, **47**, 558-561.
2. G. Kresse, et al., *Phys. Rev. B.*, 1996, **54**, 11169-11186.
3. J. P. Perdew, et al., *Phys. Rev. Lett*., 1996, **77**, 3865-3868.
4. K. Niu, et al., *J. Phys. Chem. C*, 2019, **123**, 4969-4976.
5. G. Henkelman, et al., *J. Chem. Phys.*, 2000, **113**, 9901-9904.
6. F. Liang, et al., *ACS Appl. Mater. Interfaces.*, 2021, **13**, 25523-25532.